Optimal cold bending of laminated glass

Laura Galuppi,
Gianni Royer-Carfagni[1]

Department of Industrial Engineering
University of Parma, Parco Area delle Scienze 181/A, I 43100 Parma, Italy
tel: +39-0521-905896, fax: +39-0521-905705
email: laura.galuppi@unipr.it, gianni.royer@unipr.it

Abstract

Cold-bending of laminated glass panels, by forcing their contact with a constraining frame, is a promising technique for free-form glazed surfaces. Their static state varies in time due to the viscosity of the polymeric interlayer, which causes the decay of the shear-coupling of the constituent glass plies. The direct problem consists in calculating the spatial and temporal evolution of stress after cold-bending. Considering an equivalent secant elastic shear-modulus for the interlayer to account for its viscoelasticity, various conditions for cylindrical deformations are analyzed in detail. A "conjugate-beam analogy" is proposed for the inverse problem, i.e., to determine the cylindrical deformed shape that, at a prescribed time, provides the desired state of stress. Remarkably, the simplest constant-curvature deformation, often used for cold bending, produces high shear stress concentrations in the interlayer with consequent risks of delamination. For the same sag, better linear or cubic distribution of shear stress are attained with slightly different deformations, compatibly with glass strength. Among the considered cases, the optimal configuration is sinusoidal, because it provides the smoothest distribution of shear stress with inappreciable differences with respect to the circular shape.

Keywords: Laminated glass, cold bending, sandwich beam, shape optimization, shear coupling, viscoelasticity.

[1] Corresponding author.

1. Introduction

Curved glass is a powerful tool of aesthetic design, and its use is steadily increasing in modern architecture. There are two main categories of production: hot-bending and cold-bending. Hot-bent glass is obtained by heating sheets of glass until they reach the softening point (glass transition temperature) and curving them into the desired shape against a negative form. Cold bending is a recent fabrication process that is widely developing because it allows for the construction, at relatively low cost, of curved free-form glazed surfaces with no need of negative moulds. In general, the cold bent surface is a single-curvature developable surface. Cold bending into a double curved shape is also possible (Beer 2013, Galuppi et al. 2014), but since this produces high membrane stress, single-curvature bending remains the most used technique, also because recent advances in theoretical algorithms allow for the discretization of any surface using single curvature panels only. Therefore, large double-curvature glazing of any form can be approximated by cylindrically bent panels (Pottmann et al. 2008, Eigensatz et al. 2010).

In cold bending, flat glass panels are brought to the desired geometry by external contact forces, constraining the curved glass unit in the desired shape. The most common technique[2] consists in curving glass at the construction site, holding it in place with clamps or adhesives against an underlying frame. Laminated glass is particularly adapt for cold bending. This is a sandwich structure composed by two or more glass plies bonded together by thin polymeric interlayers with a process at high temperature and pressure in autoclave. The limited shear coupling of the glass plies through the interlayer (Behr et al. 1993, Hooper 1973) reduces the overall stiffness of the panel, increasing the maximum attainable curvature through cold bending compatibly with the material strength. As pointed out by Norville et al. (1998), in general the bending stiffness of laminated glass is intermediate between the *layered limit* (free-sliding glass plies) and the *monolithic limit* (shear rigid interlayer). Since stress and strain in the monolithic limit are much lower than in the layered limit, appropriate consideration of the shear coupling offered by the interlayer is important to achieve an economical design. The problem has been considered by many authors, one of the most recent contribution being the careful finite element analysis by Ivanov (2006) that includes a list of the most relevant literature.

Due to the viscosity of the polymer, as remarked by Belis et al. (2007), the cold-bent laminated glass element exhibits a stress relaxation from the instant in which it is completely positioned in its curved frame. These effects must be precisely predicted in order to evaluate the temporal variation of the state of stress.

The shear coupling provided by the polymeric interlayer depends upon its viscoelastic response, which is highly time-dependent and temperature-dependent (Louter et al. 2010, Bennison et al. 2005, Froli and Lani 2011, Barredo et al. 2011, Galuppi and Royer-Carfagni 2012b). In the design practice it is customary to rely upon approximate solutions, the most common of which considers the polymer as a linear elastic material, characterized by a proper secant shear modulus, calibrated according to temperature and characteristic duration of the design actions (Bennison and Stelzer 2009). Such an approximation, usually referred to as the *secant stiffness* method or *quasi elastic* approximation, is equivalent to neglecting the memory effect of the viscoelastic material. This in general provides estimates on the side of safety in the case of monotone loading histories (Galuppi and Royer-Carfagni 2012b), even if there may be loading-unloading paths for which the results are not conservative, as demonstrated in Galuppi and Royer-Carfagni (2013).

Here, the single-curvature cold-bending of a laminated glass panel is analyzed. Due to the hypothesis of cylindrical deformation, the problem is tackled by using sandwich beam theory, developing a method originally proposed by Newmark et al. (1951) to evaluate the relationship between the prescribed cold-bent shape and the spatial and temporal evolution of the state of stress in both glass and polymeric interlayer. Stress relaxation is calculated by adopting the secant stiffness approximation. The model allows to solve the direct problem, i.e., to find the state of stress for any given assigned deformation of the laminated glass beam.

[2]Another technique consists in laminating a package while being constrained in the desired shape, so that after lamination it is the bond of the interlayer that keeps the assembly in the curved state. This procedure, usually denoted *cold lamination bending* (Kassnel-Henneberg 2011, de Vericourt, Fildhulth and Knippers 2011), is not considered here.

The most used shape for cold bending is constant-curvature shape. However, it will be analytically proved that such a configuration is associated with shear stress concentrations in the polymeric interlayer, possibly producing delamination as sometimes observed in the practice. The higher the shear stiffness of the interlayer, the more critical is its state of stress. In the limit case of stiff interlayers (monolithic limit), the shear stress becomes singular because concentrated forces at the extremities are necessary to guarantee equilibrium.

A "conjugate-beam analogy" is then proposed to solve the inverse problem, i.e., to determine the cold-bending shape associated with an assigned shear stress distribution in the interlayer at a prescribed time of the history. In fact, it is shown that such shape coincides with the deformation of a conjugate beam under a fictitious load and appropriate boundary conditions, which are determined by the form of the desired shear stress. Various types of shear stress distributions are analyzed in detail. Remarkably, the simplest constant-curvature shape is the one that produces the highest shear stress in the interlayer. Slightly modifying the deformation due to cold bending, better linear or cubic distributions of shear stress can be obtained. Among all the considered cases, the optimal configuration is the sinusoidal deformation, associated with a cosine distribution of shear stress in the interlayer that allows to obtain the maximum sag of the laminated package, compatibly with the strength of glass and polymer. For standard geometric parameters, the difference between the sinusoidal and the circular shapes cannot be appreciated with the naked eye, and consequently the aesthetics is not compromised. Indeed, so small differences in the constrained deformations can provide so noteworthy advantages.

2. Cold bending: mathematical model

Consider a laminated glass beam of length L and width b, composed by two glass layers of thickness h_1 and h_2 and Young's modulus E, bonded by a thin polymeric interlayer of thickness h with time-dependent shear modulus $G(t)$. Introduce a right-handed orthogonal reference frame (x, y), with x parallel to the beam axis and y directed upwards, as indicated in figure 1a. Perfect bonding between glass and polymeric interlayer is assumed and, under the hypothesis that strains are small and rotations moderate, the prescribed vertical displacement $v(x)$, assumed positive if in the same direction of increasing y, is the same for all the three layers. The *cold bending* process consists in forcing the beam to assume a curved shape. From a practical point of view, the laminated glass plate is glued or clamped along its border onto a negative curved frame, so to assume a cylindrical deformation as schematically represented in figure 1b, where the bond thickness is supposed to be negligible. In the assumed beam model, this is equivalent to assign the vertical displacement $v(x)$.

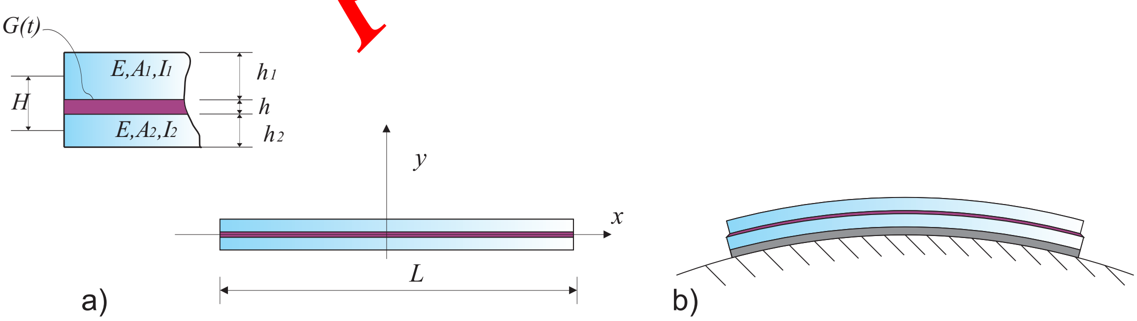

Figure 1: Laminated glass beam: a) longitudinal view and magnification of the composite package; b) Assigned deformation through cold-bending.

The viscoelasticity of the interlayer induces the relaxation of the shear coupling of the glass ply, so that the macroscopic bending stiffness of the beam varies with time. Consequently, the bending moment

$M(x,t)$ is time-dependent, as well as the constraint reaction forces per unit length $p(x,t)$. Denoting, here and further, with $'$ derivative with respect to x, and assuming that $M(x,t) > 0$ when $v''(x) > 0$, equilibrium of an elementary portion of the beam gives

$$p(x,t) = -M''(x,t)\,, \tag{2.1}$$

with $p(x,t)$ positive if directed downwards.

2.1. Viscoelasticity of the interlayer and secant-stiffness approximation

The viscoelastic properties of the interlayer[3] can be interpreted through the Maxwell-Wiechert model (see Wiechert (1893)), according to which, under constant shear-strain, the shear modulus of the viscoelastic material decays with time according to the Prony series

$$G(t) = G_\infty + \sum_{k=1}^{N} G_k e^{-t/\theta_k} = G_0 - \sum_{k=1}^{N} G_k(1 - e^{-t/\theta_k}), \tag{2.2}$$

where G_∞ is the long-term shear modulus (corresponding to the totally relaxed material), whereas the terms G_k and θ_k, $k = 1..N$, are respectively the relaxation shear moduli and the relaxation times associated with the $k-th$ Maxwell element. The instantaneous shear modulus G_0 is thus given by $G_\infty + \sum_{k=1}^{N} G_k$. Temperature dependence may be taken into account by using the Williams-Landel-Ferry model (Williams et al. 1955). Parameters that define the Prony series are seldom furnished by the producer, but they can be directly measured (Bennison and Stelzer 2009).

In general, the stress in the interlayer depends upon the whole strain history (Galuppi and Royer-Carfagni 2012b), but a very popular practical approach consists in adopting the *secant stiffness* approximation, according to which the polymer behaves as a linear elastic material, whose elastic shear modulus depends upon temperature and characteristic duration of the design actions. As discussed by Galuppi and Royer-Carfagni (2012b; 2013), this is equivalent to assume that the stress $\tau(x,t)$ in the interlayer is a linear function of the shear strain $\gamma(x,t)$ according to an expression of the form

$$\tau(x,t) = G(t)\gamma(x,t)\,, \tag{2.3}$$

where $G(t)$ is the shear modulus. The use of such an approximation is particularly effective because there are several practical methods to readily calculate the response of laminated structures composed of linear elastic layers.

In general $G(t)$ can be found from an expression of the type (2.2), but more practically the shear modulus of the polymer is provided by manufactures in tables, as a function of environmental temperature and characteristic duration of the applied shear distortion. Table 1 reports typical values of $G(t)$ for PVB at 20°C, obtained through creep tests at constant shear strain, by measuring the shear stress as a function of time.

2.2. Governing equations for the equilibrium of a laminated glass beam

With reference to Figure 1a, let us define

$$A_i = h_i b,\; I_i = \frac{bh_i^3}{12}\; (i = 1,2),\;\; H = h + \frac{h_1 + h_2}{2},\; A^* = \frac{A_1 A_2}{A_1 + A_2},\; I_{tot} = I_1 + I_2 + A^* H^2. \tag{2.4}$$

[3] There are essentially three main commercial polymeric films: Polyvinyl Butyral (PVB), Ethylene Vinyl Acetate (EVA), and ionoplast (Bennison et al. 2001). For cold bending, it is convenient to use a soft interlayer, to diminish the shear coupling of the glass plies and thus reduce the bending stiffness of laminated glass. For this reason, one of the best choice is certainly PVB, a polyvinyl acetate with addition of softeners that provide plasticity and toughness, enhancing adhesion-strength and increasing glass transition temperature up to $20-25$°C.

t	$G(t)$ [MPa]
3 seconds	8.06
1 hour	0.840
1 day	0.508
1 year	0.266
$t \to \infty$	0.052

Table 1: Time dependence for the shear modulus of a particular type of PVB at 20°C.

Clearly, I_{tot} represents the moment of inertia of the cross sections of the external layers properly spaced by the interlayer gap (Galuppi and Royer-Carfagni 2012a). As demonstrated in Galuppi and Royer-Carfagni (2012a), if strains and rotations are small, the kinematics is completely described by the vertical displacement $v(x)$, the same for the two glass components, and the horizontal displacements $u_1(x,t)$ and $u_2(x,t)$ of the centroid of the upper and lower glass element, respectively. Observe that the vertical displacement does not depend on time because the beam is fixed to the curved frame, whereas the horizontal displacements, which are affected by the shear coupling through the interlayer, can vary with time due to its viscoelastic response.

2.2.1. First variation of the strain energy

Let us suppose that, at each instant t, the beam is bent under the action of the forces per unit length $p(x,t)$ to assume the shape $v(x)$. The shear strain in the interlayer is (Galuppi and Royer-Carfagni 2012a)

$$\gamma(x,t) = \frac{1}{h}[u_1(x,t) - u_2(x,t) + v'(x)H] , \tag{2.5}$$

so that, under the quasi-elastic approximation, the strain energy of the beam $-L/2 \le x \le L/2$ at the instant t can be written in the form

$$\begin{aligned}\mathfrak{E}[u_1(x,t), u_2(x,t), v(x)] = \\ \int_{-L/2}^{L/2} \Bigg\{ \frac{1}{2}\Big[E(I_1+I_2)[v''(x)]^2 + EA_1[u_1'(x,t)]^2 + EA_2[u_2'(x,t)]^2 \\ + \frac{Gb}{h}(u_1(x,t) - u_2(x,t) + v'(x)H)^2\Big] + p(x,t)\, v(x)\Bigg\} dx\,.\end{aligned} \tag{2.6}$$

Here, the first term represents the bending of the glass plies, the second and the third terms are the extensional strain energy of the upper and lower glass ply, respectively, the fourth term corresponds to the strain energy of the interlayer whereas, recalling that $p(x,t)$ and $v(x)$ have opposite positive directions, the last term is the potential of the external loads. For fixed t, the zeroing of the first variation of the functional with respect to the variations $v(x) + \delta v(x)$, $u_1(x,t) + \delta u_1(x,t)$ and $u_2(x,t) + \delta u_2(x,t)$ gives the Euler's equilibrium equations

$$\begin{aligned} &E(I_1+I_2)v''''(x) - GbH\gamma'(x,t) + p(x,t) = 0\,, \\ &EA_1 u_1''(x,t) = Gb\gamma(x,t)\,, \\ &EA_2 u_2''(x,t) = -Gb\gamma(x,t)\,. \end{aligned} \tag{2.7}$$

As discussed in (Galuppi and Royer-Carfagni 2012a), condition $(2.7)_1$ is the equilibrium in the y-direction of a beam with inertia $I_1 + I_2$ under the external load $p(x,t)$ and under a distributed couple per unit length $m^*(x,t) = -GbH\gamma(x,t)$, which represents the stiffening contribution of the interlayer.

Standard arguments in the calculus of variation furnish the boundary conditions

$$
\begin{aligned}
&\Big[(-E(I_1+I_2)v'''(x)+GbH\gamma(x,t))\delta v(x)\Big]_{-L/2}^{L/2}=0\,,\\
&\Big[E(I_1+I_2)v''(x)\delta v'(x)\Big]_{-L/2}^{L/2}=0\,,\\
&\Big[EA_1u_1'(x,t)\delta u_1(x,t)\Big]_{-L/2}^{L/2}=0\,,\\
&\Big[EA_2u_2'(x,t)\delta u_2(x,t)\Big]_{-L/2}^{L/2}=0\,.
\end{aligned}
\tag{2.8}
$$

The terms $\delta v(x)$, $\delta u_1(x,t)$ and $\delta u_2(x,t)$ are null at the boundary where the displacement is prescribed, and arbitrary otherwise. In general, at the beam ends the horizontal displacements are not constrained, so that $\delta u_i(\pm L/2,t)\neq 0\,, i=1,2$, implying that the axial forces $N_i(x,t):=EA_iu_i(x,t)$ are null at the boundaries. The quantity appearing in $(2.8)_1$ may be regarded as a fictitious shear force

$$
V^*(x,t)=\big(-E(I_1+I_2)v'''(x)+GbH\gamma(x,t)\big)\,, \tag{2.9}
$$

accounting for the effects of the distributed moment *per* unit length due to the shear stress transferred by the interlayer.

2.2.2. Newmark's approach

An effective analytical model for a structure made of two beams with elastic shear-coupling was proposed in 1951 by Newmark et al. (1951), and applied to the case of steel-concrete composite bridge beam. The method allows to write the equilibrium equation $(2.7)_1$ as a function of the vertical displacement $v(x)$ for those cases in which the overall bending moment in the beam is known, i.e., the beam is statically determined.

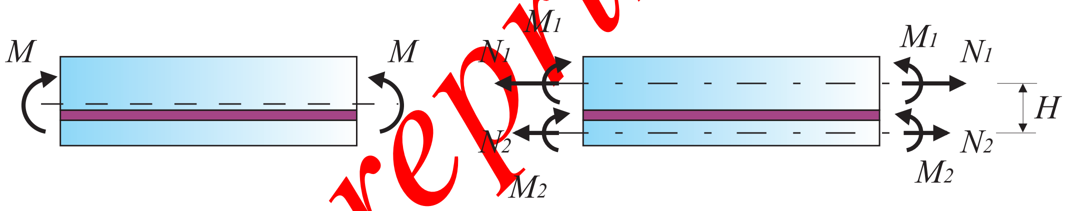

Figure 2: Schematic representation of the internal actions in a sandwich beam.

As schematically shown in Figure 2, the overall bending moment in the beam, $M(x,t)$, is due to the sum of the bending moments $M_i(x)=EI_iv''(x)$, $i=1,2$, of the i-th glass ply, and the contribution due to the axial forces $N_i(x,t)=EA_iu_i'(x,t)$, $i=1,2$, multiplied by the corresponding level arm H. Following the same argument exposed in (Galuppi and Royer-Carfagni 2012a), if no external axial forces are acting at the beam ends one can demonstrate that $N_1(x,t)=-N_2(x,t)$ and, hence, that

$$
M(x,t)=E(I_1+I_2)v''(x)-N_1(x,t)H=E(I_1+I_2)v''(x)+N_2(x,t)H\,. \tag{2.10}
$$

It is then possible to find the expressions for the axial strains $u_i'(x,t)$, $i=1,2$, in the form

$$
u_1'(x,t)=\frac{1}{HA_1}\Big[(I_1+I_2)v''(x)-\frac{M(x,t)}{E}\Big],\quad u_2'(x,t)=\frac{1}{HA_2}\Big[-(I_1+I_2)v''(x)+\frac{M(x,t)}{E}\Big]. \tag{2.11}
$$

These, together with equation (2.3) and (2.5), lead to the relationship

$$
\tau'(x,t)=G(t)\gamma'(x,t)=\frac{G(t)}{hA^*H}\Bigg[I_{tot}v''(x)-\frac{M(x,t)}{E}\Bigg]. \tag{2.12}
$$

By rearranging this equation, one finds

$$\tau'(x,t)=\frac{G(t)}{hA^*}\Bigg[HA^*v''(x)+\frac{N_1(x,t)}{E}\Bigg]=\frac{G(t)}{hA^*}\Bigg[HA^*v''(x)-\frac{N_2(x,t)}{E}\Bigg], \tag{2.13}$$

which is a noteworthy explicit relationship between the axial forces in the glass plies and the shear stress transmitted through the interlayer.

By substituting (2.12) in $(2.7)_1$ and recalling (2.1), the first equilibrium equation can be written in the form

$$E(I_1+I_2)v''''(x,t)-\frac{bI_{tot}G(t)}{hA^*}v''(x)+\frac{bG(t)}{hEA^*}M(x,t)-M''(x,t)=0\,, \tag{2.14}$$

which represents Newmark's equation.

Moreover, using (2.10) and recalling (2.9), the boundary conditions (2.8) may be re-written as

$$\begin{aligned}
&\Big[V^*(x,t)\delta v(x)\Big]_{-L/2}^{L/2}=0\,,\\
&\Big[E(I_1+I_2)v''(x)\delta v'(x)\Big]_{-L/2}^{L/2}=0\,,\\
&\Big[\tfrac{1}{H}\Big(E(I_1+I_2)v''(x)-M(x,t)\Big)\delta u_1(x)\Big]_{-L/2}^{L/2}=0\,,\\
&\Big[\tfrac{1}{H}\Big(-E(I_1+I_2)v''(x)+M(x,t)\Big)\delta u_2(x)\Big]_{-L/2}^{L/2}=0\,.
\end{aligned} \tag{2.15}$$

For the case in which the horizontal displacements are not constrained at the beam's ends, $M(\pm L/2,t)=E(I_1+I_2)\,v''(\pm L/2)$, $\forall t$.

It is also important to observe that (2.12) allows to write Newmark's equation (2.14) as a function of the shear stress $\tau(x,t)$ in the interlayer in the form

$$-EH^2A^*v''''(x,t)-bH\tau'(x,t)+\frac{EhHA^*}{G(t)}\tau'''(x,t)=0\,, \tag{2.16}$$

where H^2A^* represents the difference between the moment of inertia I_{tot}, corresponding to the the monolithic limit, and the sum of the moments of inertia of the two composing glass plies I_1+I_2, associated with the layered limit. In other words, this equation emphasizes the increase of bending stiffness due to the shear coupling of the glass plies.

If one uses (2.13), boundary conditions (2.8) may be rewritten as

$$\begin{aligned}
&\Big[V^*(x,t)\delta v(x)\Big]_{-L/2}^{L/2}=0\,,\\
&\Big[E(I_1+I_2)v''(x)\delta v'(x)\Big]_{-L/2}^{L/2}=0\,,\\
&\Big[EH^2A^*\Big(v''(x)-\tfrac{h}{HG(t)}\tau'(x,t)\Big)\delta u_1(x)\Big]_{-L/2}^{L/2}=0\,,\\
&\Big[EH^2A^*\Big(-v''(x)+\tfrac{h}{HG(t)}\tau'(x,t)\Big)\delta u_2(x)\Big]_{-L/2}^{L/2}=0\,.
\end{aligned} \tag{2.17}$$

Observe, then, that whenever the horizontal displacements are not constrained at the beam's ends, then $\tau'(\pm L/2,t)=\frac{G(t)H}{h}v''(\pm L/2)$.

2.2.3. *Conjugate-beam analogy. Cold-bending shape-optimization problem*

It is useful to provide an analogy to interpret equation (2.16), relating the shear stress with the vertical displacement of the sandwich beam. In fact, such an equation is identical to the load-deflection differential equation for a *conjugate* Euler-Bernoulli beam, with moment of inertia $\tilde{I}$, subject to a fictitious distributed load $\tilde{q}(x)$, which reads

$$E\tilde{I}v''''(x) + \tilde{q}(x) = 0\,, \quad \tilde{q}(x) = \frac{\tilde{I}}{H^2A^*}\Big[bH\tau'(x,t) - \frac{EhHA^*}{G(t)}\tau'''(x,t)\Big]\,. \tag{2.18}$$

Clearly, the deformation does not depend upon $\tilde{I}$ and one can pose, without loosing generality, $\tilde{I} = H^2A^*$. The boundary conditions for such a beam come from (2.17) and will be discussed in the examples proposed in the following sections.

From this equation, one should observe that although the shear stress $\tau(x,t)$ may vary with time due to the viscoelasticity of the interlayer, in order to satisfy (2.18) the shear stress distribution must be such that the fictitious load $\tilde{q}(x)$ is time-independent for any assigned shape $v(x)$. Furthermore, $\tilde{q}(x)$ inherits the same regularity of $v''''(x)$.

This *conjugate-beam analogy* can be useful to tackle two types of problems for the cold bending of laminated glass.

- The *direct problem* consists in determining the time-dependent shear-stress distribution $\tau(x,t)$ due to the cold bending process for any given shape of the constraint, i.e., for any given prescribed displacement $v(x)$. Once the fictitious distributed load $\tilde{q}(x)$ that causes the assigned deflection has been found from $(2.18)_1$, the corresponding shear stress $\tau(x,t)$ can be obtained by integrating, for any assigned time t, the differential equation $(2.18)_2$, with appropriate boundary conditions (2.17).

- The *inverse problem* consists in finding the shape of the constraint that, at the prescribed time t, provides the desired distribution of shear stress $\tau(x,t)$ in the interlayer. This is a problem of *structural optimization*, where one is interested in the best cold-bending shape that is compatible with the strength of materials, taking full advantage of the mechanical properties of the interlayer. To solve this *cold-bending shape-optimization problem*, equation (2.18) may be directly used. The desired vertical displacement $v(x)$ coincides with deformed shape of the conjugate beam, loaded by $\tilde{q}(x)$ calculated through $(2.18)_2$ according to the *a priori* assumed distribution $\tau(x,t)$ of shear stress. The relevant boundary conditions come from (2.17) and will be discussed in detail in Section 4.

The resulting bending moment $M(x,t)$ in the laminated glass beam may be obtained from equation (2.12) once the distribution of shear stress $\tau(x,t)$ is known. Alternatively, one can consider the differential equation (2.14), with boundary conditions (2.15), which is the counterpart of (2.18). Once the vertical displacement and the bending moment are known, recalling equation (2.10) the maximum normal stress σ_i in the $i-th$ glass ply, $i = 1, 2$, can be readily evaluated through the expressions derived in (Galuppi and Royer-Carfagni 2013) and reads

$$\begin{aligned} |\sigma_i(x,t)| &= \left|\frac{N_i(x,t)}{A_i} \pm \frac{M_i(x,t)}{I_i}\frac{h_i}{2}\right| \\ &= \left|\frac{M(x,t) - E(I_1+I_2)v''(x)}{HA_i} \pm E\frac{h_i}{2}v''(x)\right|\,. \end{aligned} \tag{2.19}$$

The contact forces transmitted by the constraints to the laminated glass beam coincide with the distributed load $p(x,t)$, calculated from (2.1). Of course the order of the relevant differential equations confirm that in the case of symmetric bending, i.e., symmetric vertical displacement, the distribution of shear stress is antisymmetric.

3. Direct problem

In the *direct problem* the cold-bending shape $v(x)$ is fixed and the time-dependent shear stress distribution $\tau(x,t)$ needs to be found.

3.1. Constant-curvature cold bending

The most common shape used for cold-bending is certainly that where the radius of curvature ρ, and hence the curvature $K := 1/\rho$, is constant (Fildhuth and Knippers 2014, Fildhuth et al. 2014, Belis et al. 2007). Based upon the assumption of small strains and rotations, in the present model the arc of the circle is approximated by a parabola because $K \simeq v''(x)$. In Figure 3 a graphical comparison is made between a parabolic deformed shape with $v'' = -10^{-4}$ mm^{-1}, and an arc with (constant) curvature $K = -10^{-4}$ mm^{-1}, for a beam of length of 2400 mm. It is evident that for the assumed values, which are typical of a practical situation, the two curves are indistinguishable: $v_{max} = 72$ mm for the parabola and $v_{max} = 72.26$ mm for the arc.

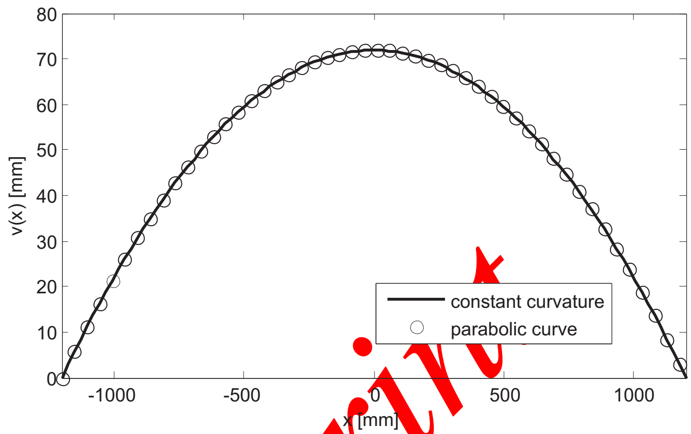

Figure 3: Comparison between a parabolic deformed shape and an arc of a circle.

As an illustrative example, consider the constant-curvature cold-bending of a beam of length $L = 2400$ mm, width $b = 800$ mm, composed by two glass plies of thickness $h_1 = h_2 = 6$ mm and Young's modulus $E = 70000$ MPa, bonded by a PVB interlayer of thickness $h = 1.52$ mm and shear modulus $G(t)$. This is the same geometry considered by Fildhuth and Knippers (2014). According to the small strain hypothesis, the equation of the imposed displacement is $v(x) = \frac{K}{2}\left(x^2 - \frac{L^2}{4}\right)$ with $K = -10^{-4}$ mm^{-1}, and its graph is plotted in Figure 3.

From the conjugate beam method governed by equation (2.18), one finds that the fictitious distributed load $\tilde{q}(x)$ that causes the prescribed deflection of the beam is null because

$$\tilde{q}(x) = \frac{\tilde{I}}{H^2 A^*}\left[bH\tau'(x,t) - \frac{EhHA^*}{G(t)}\tau'''(x,t)\right] = E\tilde{I}v''''(x) = 0\,. \tag{3.1}$$

The time-dependent shear stress distribution due to the cold bending process may be found by solving the differential equation ot the third order (3.1). Since no axial force is applied at the beam extremities, in $(2.17)_{3-4}$ one has that $\delta u_1(x,t)$ and $\delta u_2(x,t)$ are arbitrary, so that $\tau'(\pm L/2, t) = KHG(t)/h$. Moreover, since by symmetry and equilibrium $\int_{-L/2}^{L/2} \tau(x,t)dx = 0$, $\forall t$, one finds the expression

$$\tau(x,t) = \frac{\beta(t)EA^*HK}{b}\frac{\sinh(\beta(t)x)}{\cosh(\beta(t)L/2)}\,, \quad \beta(t) := \sqrt{\frac{bG(t)}{EhA^*}}\,. \tag{3.2}$$

Assuming for $G(t)$ the values from Table 1, plots of $\tau(x,t)$ for various values of t, i.e., for different time after the forcing of the beam in the desired position, are shown in Figure 4 as a function of x. The instant $t = 3$ s corresponds to the time that is usually required to position the glass element on the curved constraining frame. What should be noticed here is that, whereas the long-term behavior entails low values of the shear stress in the interlayer, in the short-term (high values of $G(t)$) the shear stresses tend to concentrate in the neighborhood of the beam ends.

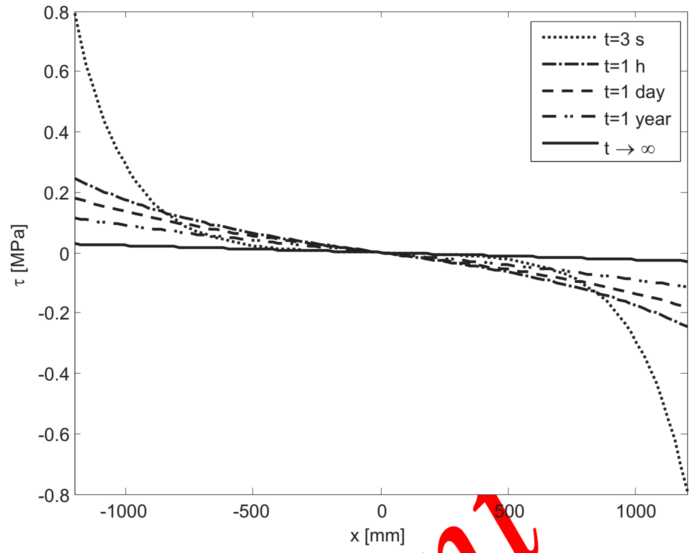

Figure 4: Constant-curvature cold bending; coupling shear stress transmitted by the interlayer for various times.

Such an high level of required shear stress can hardly be supported by the interlayer, and risk of delamination is high. Indeed, recent experimental tests by Fildhuth and Knippers (2014) seem to confirm this finding.

Analytically, it can be verified that

$$\begin{aligned}&\lim_{G(t)\to 0} \tau(x,t) = \lim_{\beta(t)\to 0} \tau(x,t) = 0\,;\\&\lim_{G(t)\to\infty} \tau(x,t) = \lim_{\beta(t)\to\infty} \tau(x,t) = \begin{cases}\infty & x=-L/2\,;\\ 0 & |x|<L/2\,;\\ -\infty & x=L/2\,.\end{cases}\end{aligned} \tag{3.3}$$

This means that when the monolithic limit is attained, i.e., when $G(t)\to\infty$ and no relative slippage occurs between glass plies, cold-bending with constant curvature implies the occurrence of concentrated shear forces F in the interlayer, at the beam extremities. The force F acting at $x=-L/2$ can be evaluated as

$$F = \lim_{\beta(t)\to\infty}\int_{-L/2}^{0} \tau(x,t) = -EA^*HK \lim_{\beta(t)\to\infty} \frac{\cosh(\beta(t)L/2)-1}{\cosh(\beta(t)L/2)} = -EA^*HK\,. \tag{3.4}$$

This somehow intriguing finding will be discussed in Section 3.2.

The bending moment $M(x,t)$ and the maximum axial stress $\sigma_{max}(t) := \max_{x,i} \sigma_i(x,t)$ may be evaluated by using (2.12) and (2.19), and read

$$\begin{aligned}M(x,t) &= EI_{tot}K - \frac{EhA^*H^2}{\beta(t)}\frac{\cosh(\beta(t)x)}{\cosh(\beta(t)L/2)}\,,\\ \sigma_{max}(t) &= \left|EK\left[\frac{A^*H(cosh(\beta(t)L/2)-2)}{A_i cosh(\beta(t)L/2)} \pm \frac{h_i}{2}\right]\right|\,.\end{aligned} \tag{3.5}$$

It should be observed that, at the monolithic limit, $\lim_{\beta(t)\to 0} M(x,t) = EI_{tot}K$, which represents the (constant) bending moment acting on a monolithic beam with curvature K and moment of inertia I_{tot}.

Figure 5 shows plots of the bending moment and the maximum axial stress $\sigma_{max}(t)$ for different times after having been forced on the constraining profile.

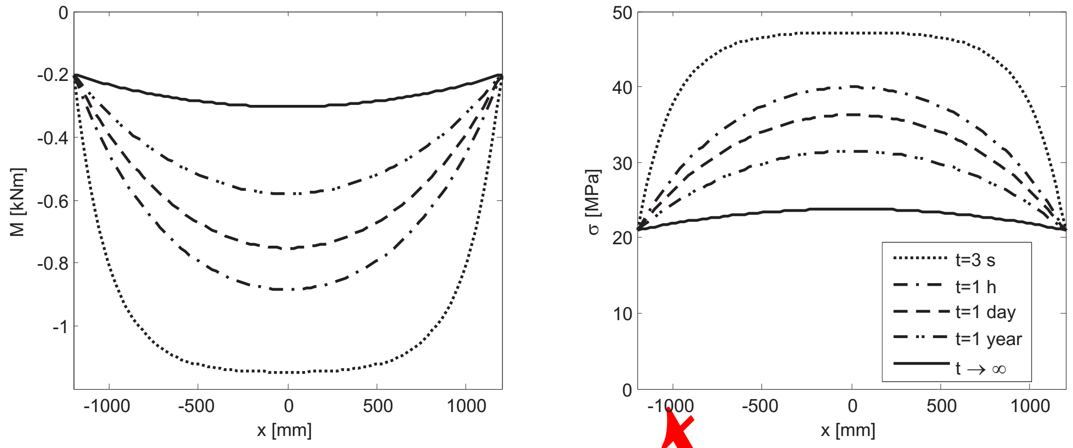

Figure 5: Constant-curvature cold bending; a) bending moment and b) maximum axial stress in the glass plies.

In order to evaluate the accuracy of the proposed method, the obtained results, in terms of both shear stress transmitted by the interlayer and axial stress in the glass plies, have been compared with an accurate numerical analysis. Simulations have been made with the FEM code ABAQUS, using a 3-D mesh with solid 20-node quadratic bricks with reduced integration, available in the program library (ABAQUS 2010). Linear elasticity is used for all materials, considering the appropriate secant stiffness of the polymer in agreement with the quasi elastic approximation. The structured mesh has been created by dividing the width of the beam in 20 elements, the thickness of each glass ply in 3 elements and the thickness of the interlayer in 2 elements. The mesh has been refined in the neighborhood of the beam ends to allow a correct estimate of the shear stress in this zone. In order to simulate the cold-bending, the out-of-plane displacement of the surface of the composite package is constrained to follow a parabolic profile.

Figures 6a and 6b show the comparison between numerical and analytical results for, respectively, the shear stress transmitted across the PVB interlayer (evaluated through equation (3.2)) and the axial stress in the glass plies (equation $(3.5)_2$). Comparisons are made for $t = 3$ s, corresponding to $G = 8.06$ MPa and $t = 1$ day, for which $G = 0.508$ MPa. It is evident that the proposed method provides very accurate results.

In the *secant stiffness* approximation, the shear stress relaxation coincides with the time-dependent shear modulus $G(t)$ calculated according with the Prony's series (2.2). Using the coefficients furnished by Bennison and Stelzer (2009), Figure 7 shows the maximum shear stress in the interlayer $\tau_{max}(t) := \max_x \tau(x,t)$, as well as the maximum axial stress in the glass plies, as a function of time t for $t > 3$ s, which represents the time assumed to be necessary to force the laminate onto the constraining frame.

3.2. On the occurrence of concentrated shear forces at the monolithic limit

Consider a laminated glass beam with a shear-rigid interlayer ($G(t) \to \infty$), cold bent with constant curvature ($K = v''(x) = const$). The coupling of the glass plies is due to the distribution of shear stresses $\tau(x)$, shown in Figure 8a, which is related with the axial force $N_i(x)$, $i = 1, 2$, in the $i - th$ glass ply through the equations of horizontal equilibrium $(2.7)_{2-3}$, implying that

$$N_1(x) = -N_2(x) = \int_0^x \tau(r)\, dr\,. \tag{3.6}$$

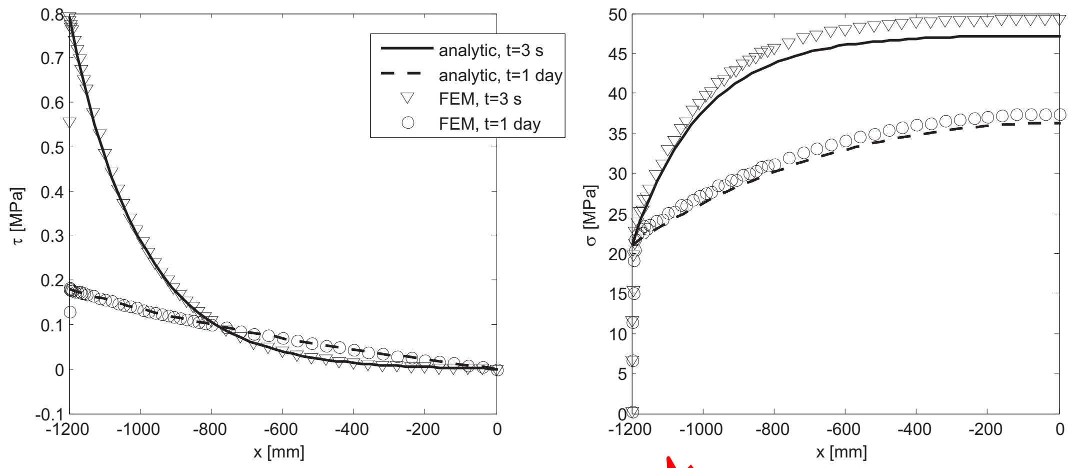

Figure 6: Constant-curvature cold bending. Comparisons of the analytical and numerical results in terms of a) shear stress transmitted by the interlayer and b) maximum axial stress in the glass plies.

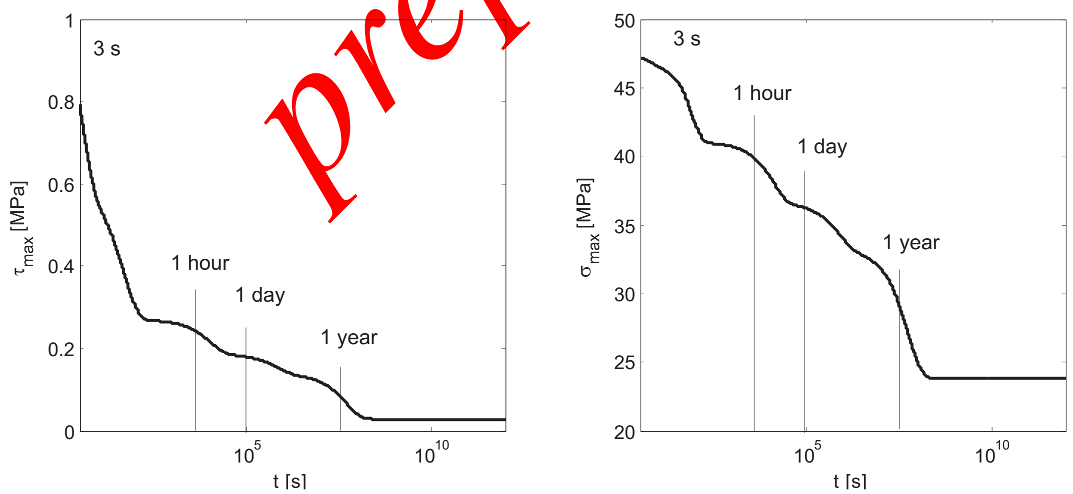

Figure 7: Constant-curvature cold bending. Evolution in time of the maximum shear stress (in the interlayer) and the maximum axial stress (in the glass plies).

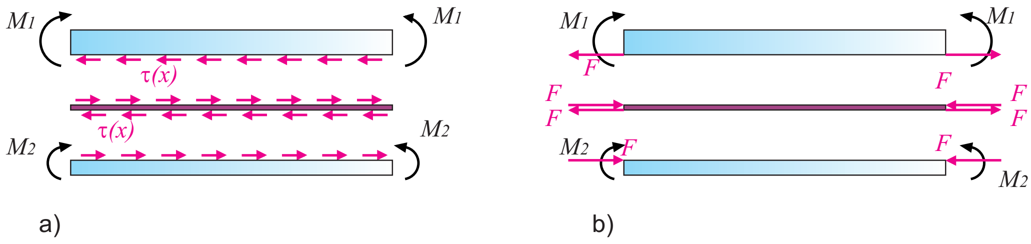

Figure 8: Shear stresses transmitted by the interlayer: a) continuous shear stress distribution, b) singular stress distribution associated with concentrated forces at the beam ends.

When the monolithic limit is attained, the moment of inertia of the beam is I_{tot} and the bending moment is $M(x) = EI_{tot}K = const$. On the other hand, by requiring that the two glass plies have the same vertical displacement and, hence, the same curvature, one has $\frac{M_1(x)}{EI_1} = \frac{M_2(x)}{EI_2} = K = const$. Recalling relation (2.10), it is evident that the axial forces must be constant, that is

$$N_1(x) = -N_2(x) = -\frac{M(x) - M_1(x) - M_2(x)}{H} = const\,, \quad \Rightarrow \int_0^x \tau(r)\,dr = const\,. \tag{3.7}$$

Since from the boundary conditions $(2.8)_{3-4}$ one finds $N_i(\pm L/2) = 0$, $i = 1, 2$, equation (3.7) would imply that the shear stress distribution along the beam is null. However, the solution $\tau(x) = 0\ \forall x$ would lead to the paradoxical conclusion of null shear coupling offered by the interlayer and to

$$N_1(x) = -\frac{M(x) - M_1(x) - M_2(x)}{H} = -\frac{E(I_{tot} - I_1 - I_2)K}{H} = 0\,. \tag{3.8}$$

This means that the proposed solution is not compatible with the condition of equal vertical displacement of the glass plies. This condition requires the existence of shear coupling through the interlayer, but at the same time this has to be null almost everywhere for $x \in (-L/2, L/2)$. Therefore, the only possibility is to assume the occurrence of concentrated shear forces F in correspondence of the beam ends, as represented in Figure 8b.

¿From equilibrium, it is easy to show that

$$N_1(x) = -N_2(x) = F\,, \quad \Rightarrow F = -\frac{M(x) - M_1(x) - M_2(x)}{H} = -EHA^*K\,. \tag{3.9}$$

This conclusion is in agreement with equation (3.4).

4. Inverse problem and shape optimization

The *inverse problem* consists in finding the deformed shape in the cold-bending process that leads to a desired distribution of the shear stress in the interlayer. Before starting the analytical study of this issue, a few comments need to be made.

First of all, observe that for any constrained shape of the beam, fixed in time, the shear stress in the interlayer is time-dependent because of its viscoelastic properties. In order to satisfy (2.18), it is thus necessary that the shear stress distribution maintains the fictitious load $\tilde{q}(x)$ constant in time. Hence, it is not possible to prescribe both the spatial and time dependence of the shear stress $\tau(x,t)$, but only its spatial distribution at a given time t. The temporal evolution of the shear stresses is governed by the time dependence of the shear modulus $G(t)$, evaluated according to (2.2), but it must be such to assure that the fictitious load $\tilde{q}(x)$ does not vary in time.

The stress in the laminated glass beam may vary during its lifetime. Since the main goal is certainly to control the long-term behavior of laminated glass, the optimization of the shear stress in the interlayer should be done for the condition in which the polymer is almost totally relaxed, i.e., for $G(t) \to G_\infty$. To distinguish this stage, the corresponding stress distribution will be denoted in the sequel as $\overline{\tau}_\infty(x) := \lim_{t\to\infty} \tau(x,t)$, so that the fictitious load of (2.18) becomes

$$\tilde{q}(x) = \frac{\tilde{I}}{H^2 A^*}\left[bH\overline{\tau}'_\infty(x) - \frac{EhHA^*}{G_\infty}\overline{\tau}'''_\infty(x)\right]. \tag{4.1}$$

In any case, the forthcoming considerations could also be applied to control the shear stress at any instant of the panel lifetime. Apart from the long-term situation, it would be also of interest to verify the shear stress immediately after the cold-bending procedure, when the shear modulus of the interlayer is the highest.

Once the shear distribution for the assumed value of $G(t)$ have been fixed, from the beam-analogy of Section 2.2.3 the vertical constraining displacement $v(x)$ coincides with the deformed shape of the conjugate beam under the fictitious load given by (2.18), or (4.1) for $t \to \infty$. The corresponding boundary conditions for the vertical displacement, which are defined by (2.8), not necessarily coincide with boundary condition of the laminated glass beam under consideration[4].

Four different-in-type spatial distributions of the shear stresses (hyperbolic sinusoidal, linear, cubic and sinusoidal), will be considered. As it is clear from Figure 9, the deformed shapes that will result from such distributions are very close one-another, but the corresponding shear stress in the interlayer will be much different.

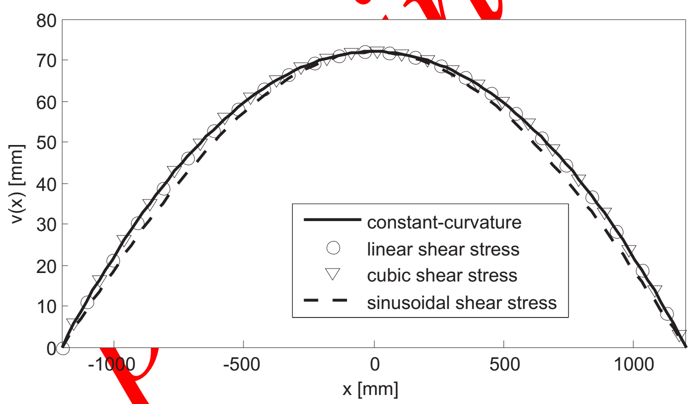

Figure 9: Comparison among the deformed shapes of the beam for different-in-type distributions of the shear stress, maintaining the same maximum displacement.

4.1. *Validation. Hyperbolic sinusoidal distribution of shear stress*

The hyperbolic sinusoidal distribution of shear stress is of the same type found in the direct problem of Section 3.1 for the case of constant curvature, and it is now considered for the sake of validating that result. Consider then the distribution

$$\overline{\tau}_\infty(x) = C \sinh(\beta_\infty x)\,, \tag{4.2}$$

[4]This is also true in the famous analogy of Christian Otto Mohr (1835–1918), which allows the computation of displacements and slopes in a linear elastic Euler-Bernoulli beam as bending moments and shear forces in an adjoint beam loaded by auxiliary forces and having modified support conditions (Timoshenko and MacCullough 1949).

where C is the constant representing the amplitude and $\beta_\infty := \sqrt{\frac{bG_\infty}{EhA^*}}$. The fictitious load $\tilde{q}(x)$ is null as *per* equation (4.1).

The vertical displacement of the conjugate beam under such a load satisfies

$$v''''(x) = 0 \quad \Rightarrow \quad v(x) = c_1 x^3 + c_2 x^2 + c_3 x + c_4\,, \tag{4.3}$$

where c_1, c_2, c_3 and c_4 are constants that must be determined from the boundary conditions. Observe, in passing, that if the *conjugate beam* was simply supported as the original laminated glass beam, from $v(\pm L/2) = 0$ and $v''(\pm L/2) = 0$ one would find $v(x) = 0\ \forall x$, and consequently $C = 0$ in (4.2) (null shear stress). The correct boundary conditions for the conjugate beam must be found from $(2.17)_{3-4}$, which inherit the information about the shear stress. Since $\delta u_1(x,t)$ and $\delta u_2(x,t)$ are arbitrary, one finds

$$v''(\pm L/2) = \frac{h}{HG_\infty}\bar{\tau}'_\infty(\pm L/2) = \frac{h\,C}{HG_\infty}\beta_\infty \cosh(\beta_\infty L/2)\,. \tag{4.4}$$

Moreover, imposing that $v(\pm L/2) = 0$, so to rule out the rigid body displacement, one finds from (4.3) that

$$v(x) = \frac{K}{2}\left(x^2 - \frac{L^2}{4}\right) = \frac{h\,C}{2HG_\infty}\beta_\infty \cosh(\beta_\infty L/2)\left(x^2 - \frac{L^2}{4}\right). \tag{4.5}$$

Hence, as expected, the deformation is identical to that found in the direct problem of Section 3.1. In fact, the function (4.5) coincides with (3.2) calculated for $G(t) = G_\infty$ because, recalling the expression of β_∞, one has $C = \frac{\beta_\infty EA^*HK}{b\cosh(\beta_\infty L/2)}$.

At other times of the history, the shear stress $\tau(x,t)$ must satisfy the differential equation $(2.18)_2$, with boundary conditions still given by $(2.17)_{3-4}$. The corresponding solutions coincide with those given by equation (3.2) and represented in Figure 4 and 7a. The bending moments and the axial stress in the glass plies may be evaluated by means of (2.12) and (2.19), respectively. Their values, given by equations (3.5), are plotted in Figures 5 and 7b.

4.2. Linear distribution of shear stress

Let us consider now a linear distribution of shear stress, which corresponds to a constant fictitious load, of the type

$$\bar{\tau}_\infty(x) = -\frac{2T}{L}\,x\,, \quad \Rightarrow \tilde{q}(x) = -\frac{\tilde{I}}{H^2A^*}\frac{2bHT}{L}\,, \tag{4.6}$$

where T is the maximum value of the stress.

Reasoning as in Section 4.1, the boundary conditions are $v(\pm L/2) = 0$ and, from $(2.17)_{3-4}$, $v''(\pm L/2) = -2\frac{h}{HG_\infty L}T$. Consequently, the displacement field takes the form

$$v(x) = \frac{bT}{HLEA^*}\left(\frac{x^4}{12} - \frac{L^2x^2}{24} + \frac{L^4}{192}\right) - \frac{c}{L}\left(x^2 - \frac{L^2}{4}\right), \tag{4.7}$$

where the parameter c, which represents the rotation at the beam extremities, reads $c = T\left(\frac{h}{HG_\infty} + \frac{bL^2}{12HEA^*}\right)$. The maximum displacement is $v_{max} = v(0) = T\left(\frac{hL}{4HG_\infty} + \frac{5bL^3}{192HEA^*}\right)$. For the same beam considered in Section 3 ($L = 2400$ mm, $b = 800$ mm, $h_1 = h_2 = 6$ mm, $h = 1.52$ mm), when $v_{max} = 72$ mm one finds that the maximum shear stress for $t \to \infty$ is $T = 0.028$ MPa. The deformed shape is plotted in Figure 9.

Once that the deformed shape associated with the desired distribution of shear stress at $t \to \infty$ has been found, one can solve the direct problem to calculate the evolution in time of the static state . Assigned the displacement (4.7), $\tau(x,t)$ is found through (2.18), with boundary conditions $\tau'(\pm L/2, t) = \frac{G(t)H}{h}v''(\pm L/2)$ and the equilibrium condition $\int_{-L/2}^{L/2}\tau(x,t)dx = 0$, $\forall t$, leading to

$$\tau(x,t) = -\frac{2T}{L}\,x - \frac{2T}{\beta(t)L}\,\frac{G_\infty - G(t)}{G_\infty}\,\frac{\sinh(\beta(t)x)}{\cosh(\beta(t)L/2)}\,, \quad \beta(t) := \sqrt{\frac{bG(t)}{EhA^*}}\,. \tag{4.8}$$

The corresponding plots at different times are shown in Figure 10. It should be observed that the state of stress arising at the beginning is much more severe than that appearing in the long-term.

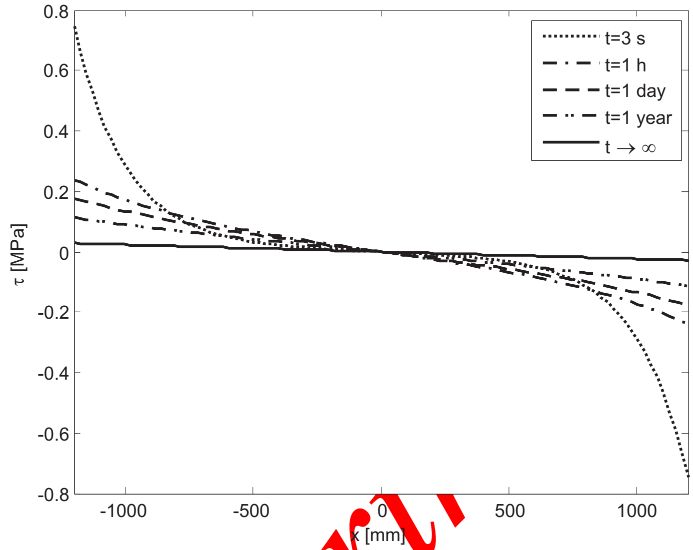

Figure 10: Bending with linear long-term shear stress. Evolution in time of the shear stress in the interlayer.

The bending moment, which can be evaluated through (2.12), or equivalently (2.14), with boundary conditions (2.15), reads

$$M(x,t) = \frac{2T}{L}\left[EHhA^*\left(\frac{1}{G_\infty} - \frac{1}{G(t)}\right)\frac{\cosh(\beta(t)x)}{\cosh(\beta(t)L/2)} + \frac{bI_{tot}}{2HA^*}\left(x^2 - \frac{L^2}{4}\right) - \frac{EhI_{tot}}{HG_\infty} + \frac{EhHA^*}{G(t)}\right], \tag{4.9}$$

where $\beta(t)$ has been defined in (4.8). The bending moment clearly varies with time according with $G(t)$ and tends to be parabolic for $G(t) \to G_\infty$. The maximum axial stress $|\sigma_i(x,t)|$ in glass is determined by (2.19). Figure 11 shows the corresponding trends at various times.

Figure 12 shows the relaxation in time of both the maximum shear stress in the interlayer $\tau_{max}(t)$ and the maximum axial stress $\sigma_{max}(t)$ in the glass plies.

4.3. Cubic distribution of shear stress

Let us assume a cubic distribution of the shear stress, varying from $\overline{\tau}_\infty(-L/2) = T$ and $\overline{\tau}_\infty(L/2) = -T$, and such that the fictitious load $\tilde{q}(x)$ is parabolic, with null values at the beam ends. In particular, let us consider

$$\begin{aligned} \overline{\tau}_\infty(x) &= \frac{T\,x}{L}\,\frac{bG_\infty(4x^2 - 3L^2) + 24EhA^*}{bG_\infty L^2 - 12EhA^*}\,, \\ \tilde{q}(x) &= \frac{\tilde{I}}{H^2A^*}\,a\left(x^2 - \frac{L^2}{4}\right), \qquad a = -\frac{12THb^2G_\infty}{bG_\infty L^2 - 12EhA^*}\,. \end{aligned} \tag{4.10}$$

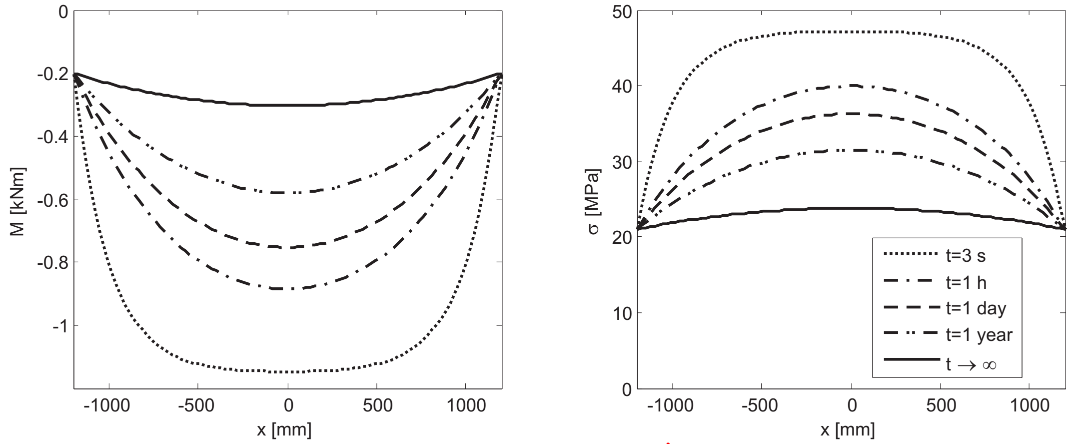

Figure 11: Bending with linear long-term shear stress. a) Bending moment and b) maximum tensile stress in the glass plies.

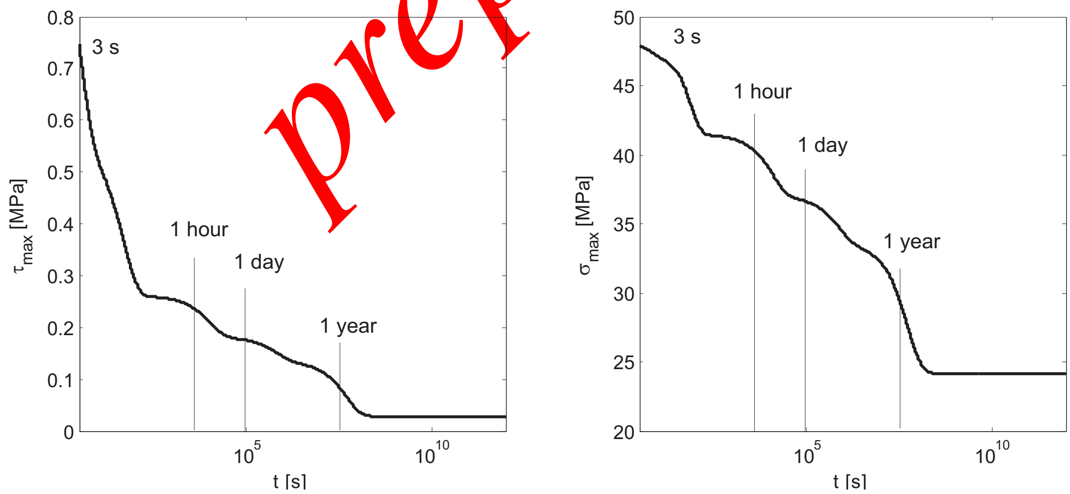

Figure 12: Bending with linear long-term shear stress. Time-evolution of maximum shear stress (in the interlayer) and maximum axial stress (in glass).

With the conjugate-beam analogy of Section 2.2.3, one finds a displacement of the form

$$v(x) = \left(x^2 - \frac{L^2}{4}\right)\left[\frac{Tb^2G_\infty}{120\,L\,EHA^*}\left(x^2 - \frac{L^2}{4}\right)(4x^2 - 13L^2) - \frac{c}{L}\right], \tag{4.11}$$

where the parameter c, which represents the rotation at the beam extremities, reads

$$c = \frac{T}{H(bG_\infty L^2 - 12EhA^*)}\left[\frac{Lb^2G_\infty}{10EA^*} - \frac{12Eh^2A^*}{G_\infty}\right]. \tag{4.12}$$

The corresponding plot for $v_{max} = 72$ mm is shown in Figure 9.

Assumed the shape (4.11), the time-dependent shear stress distribution may be found with the same procedure of the previous sections and reads

$$\begin{aligned} \tau(x,t) = {} & \frac{Tx}{L}\frac{G_\infty}{G(t)}\frac{bG(t)(4x^2 - 3L^2) + 24EhA^*}{bG_\infty L^2 - 12EhA^*} \\ & + \frac{24ThEA^*}{L\beta(t)G(t)G_\infty}\frac{G^2(t) - G_\infty^2}{bG_\infty L^2 - 12EhA^*}\frac{\sinh(\beta(t)x)}{\cosh(\beta(t)L/2)}. \end{aligned} \tag{4.13}$$

The graphs corresponding to various times are plotted in Figure 13. From the comparison of such figure with Figures 10 and 4, observe that the short-term shear stresses are quite similar one another, since they all present stress concentrations at the beam extremities.

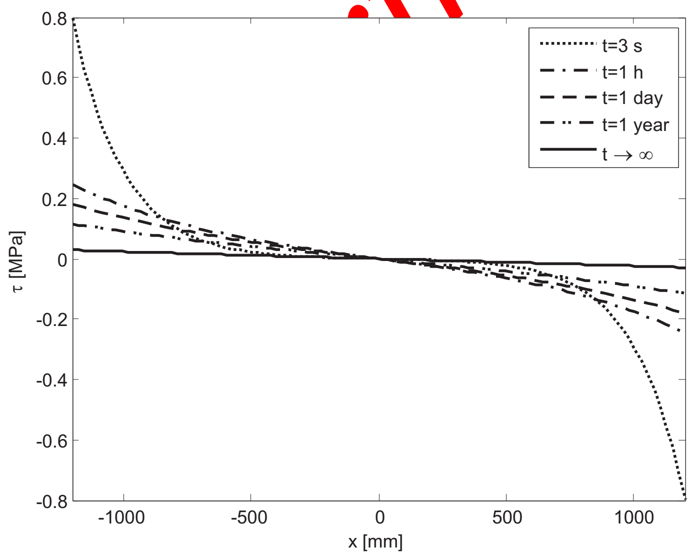

Figure 13: Bending with cubic long-term shear stress. Shear stress transmitted through the interlayer at different times.

The bending moment and the maximum axial stress, calculated according to (2.12) and (2.19), respectively, turn out to be very similar to those evaluated for the case of linear distribution of the shear stress (see Figure 11). Analoguosly, the trend of the time-decay of the maximum axial stress in the glass plies and the maximum shear stress in the interlayer is very similar to that found in the previous sections.

4.4. Sinusoidal distribution of shear stress

The last case is that of sinusoidal distribution of the shear stress that leads to a fictitious load $\tilde{q}(x)$ of the form

$$\overline{\tau}_\infty(x) = T\sin\left(\frac{\pi x}{L}\right), \quad \Rightarrow \tilde{q}(x) = \frac{I}{H^2A^*}\frac{TEhHA^*}{G_\infty}\left(\frac{bG_\infty}{EhA^*}+\frac{\pi^2}{L^2}\right)\cos\left(\frac{\pi x}{L}\right), \tag{4.14}$$

where T, again, represents the maximum value of the shear stress, occurring at the beam ends. The shape of the constraint profile can be evaluated through (2.18). This particular case is different from the other so far considered because the first derivative of $\overline{\tau}_\infty(x)$ at $x = \pm L/2$ is null, so that from $(2.17)_{3-4}$ one has $v''(\pm L/2) = 0$. Adding the condition $v(\pm L/2) = 0$, one finds that the conjugate beam is simply supported. The resulting vertical displacement reads

$$v(x) = -\frac{hT}{G_\infty H}\left(\frac{bG_\infty}{EhA^*}+\frac{\pi^2}{L^2}\right)\frac{L^3}{\pi^3}\cos\left(\frac{\pi x}{L}\right). \tag{4.15}$$

The maximum vertical displacement depends upon T according to an expression of the type

$$T = -\frac{G_\infty H}{h\left(\frac{bG_\infty}{EhA^*}+\frac{\pi^2}{L^2}\right)}\frac{\pi^3}{L^3}v_{max}. \tag{4.16}$$

A plot of (4.15) is shown in Figure 9. Indeed, all the deformations obtained in the previous sections are juxtaposed in the same picture for the same $v_{max} = 72$ mm and, from these, it is evident how limited are the differences between one another. Nevertheless, the stress distribution in both glass plies and interlayer are different in type.

For the same laminated package considered in the previous section, cold-bending according to (4.15) produces in time the shear stress distribution

$$\tau(x,t) = -\frac{TG(t)}{G_\infty}\frac{\left(\frac{bG_\infty}{EhA^*}+\frac{\pi^2}{L^2}\right)}{\left(\frac{bG(t)}{EhA^*}+\frac{\pi^2}{L^2}\right)}\sin\left(\frac{\pi x}{L}\right). \tag{4.17}$$

Figure 14 shows graphs of $\tau(x,t)$ as a function of x, for various values of t. By comparing Figure 14 with Figure 4, which represents its counterpart for the case of constant-curvature bending, observe that now there are no shear stress intensification in the neighborhood of the beam extremities, even when the shear modulus of the interlayer is quite high. Indeed, the maximum shear stress is much lower that in all the other cases considered so far.

The bending moment and the maximum axial stress in the glass plies can be evaluated through (2.12) and (2.19), which give

$$\begin{aligned} M(x,t) &= \frac{TEh}{G_\infty}\left(\frac{bG_\infty}{EhA^*}+\frac{\pi^2}{L^2}\right)\left[-\frac{EhHA^*\pi}{L\left(\frac{bG(t)}{A^*}+\frac{\pi^2}{L^2}\right)}+\frac{I_{tot}L}{H\pi}\right]\cos\left(\frac{\pi x}{L}\right), \\ \sigma_{max}(t) &= \left|E\frac{\pi^2}{L^2}\left[-\frac{bG(t)H}{EhA_i\left(\frac{\pi^2}{L^2}+\frac{bG(t)}{EhA^*}\right)}\pm\frac{h_i}{2}\right]T\frac{h\left(\frac{bG_\infty}{EhA^*}+\frac{\pi^2}{L^2}\right)}{G_\infty H}\frac{L^3}{\pi^3}\right|. \end{aligned} \tag{4.18}$$

Figure 15 shows the bending moment $M(x,t)$ and the axial stress $\sigma(x,t)$ as a function of x at different times t. Comparing Figure 15 with Figure 5, notice that for any given t the maximum axial stress in the glass plies is slightly higher in the case of cosinusoidal bending than in the case of constant curvature bending.

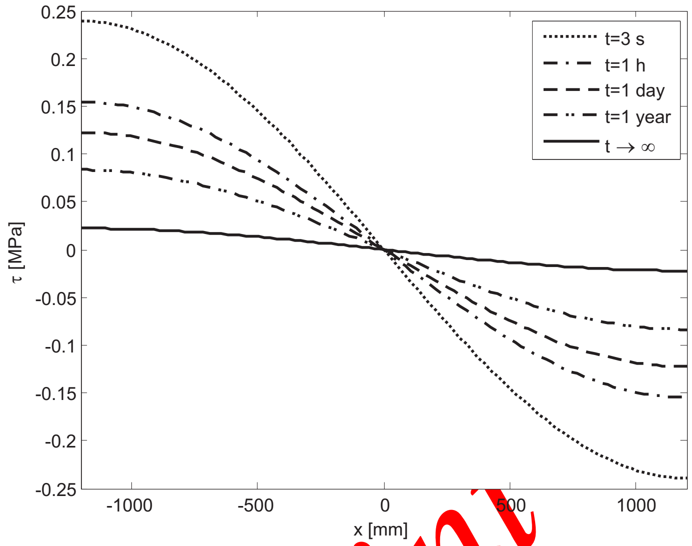

Figure 14: Cosinusoidal bending. Shear stress transmitted by the interlayer for different times.

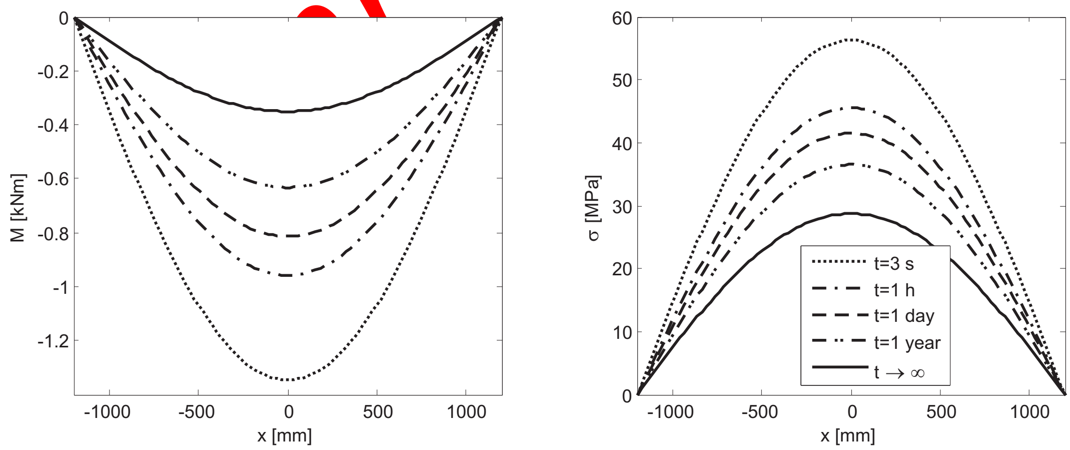

Figure 15: Cosinusoidal bending. a) Bending moment and b) maximum axial stress in the glass plies.

For example, at $t = 3$ s it is approximately 20% higher. On the other hand, the maximum shear stress in the interlayer is approximately 70% lower.

Figure 16 shows the maximum axial stress in the glass plies and the maximum shear stress in the interlayer as a functions of time.

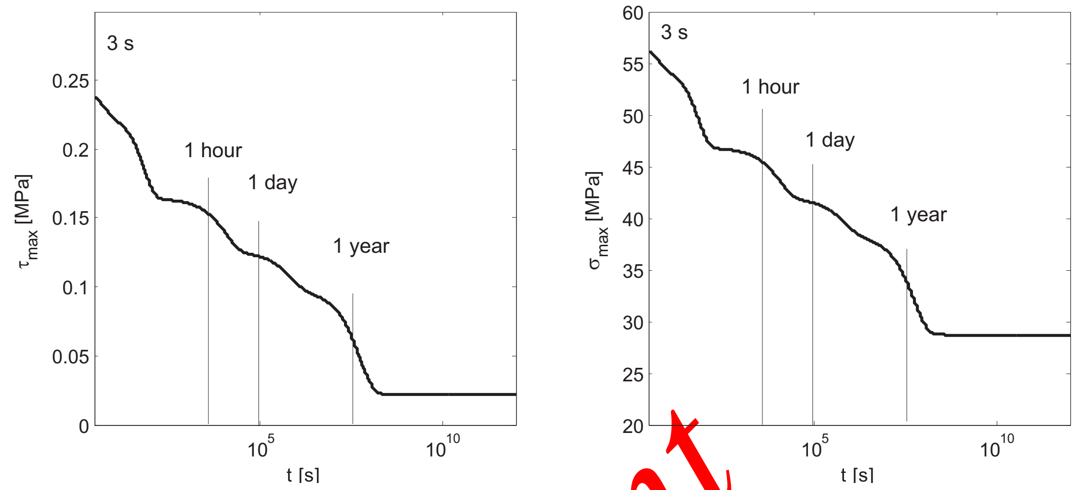

Figure 16: Cosinusoidal bending. Time-evolution of maximum shear stress (in the interlayer) and maximum axial stress (in glass plies).

5. Discussion and conclusions

The aim of this article has been to evaluate the relationship between the deformed shape of a laminated glass beam attained through a cold-bending process, and the spatial and temporal distribution of shear stress transmitted by the interlayer to the glass plies. To do so, an analytical model that develops the method originally proposed by Newmark et al. (1951) has been proposed under the classical "quasi elastic" approximation, i.e., the polymer forming the interlayer is an elastic material whose shear modulus is a function of load duration and environmental temperature.

In the practice, the most common shape that is given to glass through cold bending is certainly the one with constant curvature. However, we have shown that such a shape is perhaps one of the worst that could be selected, because very strong shear stress concentrations occur in the interlayer in the neighborhood of the beam ends. The higher is the shear modulus of the polymer forming the interlayer, the most critical is the corresponding state of stress. For a very high shear modulus of the interlayer, such that the response of laminated glass approaches the monolithic limit, cold bending with constant curvature theoretically leads to *concentrated* shear forces (infinite stress) at the ends of the beam. This may explain the delamination phenomena that may be encountered during cold bending. Of course, due to the viscosity of the polymer, the stress concentrations diminish with time, but the stress at the extremities of the beam remains much higher than at midspan.

The form of the equations governing the problem has suggested a "conjugate-beam analogy", which is very useful to solve the inverse problem: given the shear stress distribution in the interlayer, find the cold-bending shape that produces it. In fact, such a shape is the deformation of a conjugate (auxiliary) beam under a fictitious load, which depends upon the assumed distribution of shear stress only. Proper boundary conditions must be used for the conjugate beam, which are in general different from the boundary conditions for the laminated glass under consideration. This approach recalls in some ways the famous method proposed by Otto Mohr (1835-1918) to find the slope and deflection of the elastic curve by calculating the shear and bending moments diagrams in a conjugate beam with appropriate loads and boundary conditions (Timoshenko and MacCullough 1949). Of course the resulting cold-bending shape depends upon the shear modulus of the interlayer, which varies with time. Consequently, such deflection produces the assumed shear stress distribution only when the shear modulus of the interlayer takes the target value.

In other words, the shear stress in the interlayer varies with time, but the cold-bending shape can be appropriately calibrated so to produce, at a prescribed time of the element life, the desired distribution. Critical times to be checked are of course the initial stage, when the shear modulus of the polymeric interlayer is the highest, and the final long-term stage, when the shear modulus attains the lowest value. In the article we have focused on the latter condition, even if the method can be applied in exactly the same manner at any time of the history. Of course, an *optimal* distribution of shear stress is characterized by its smoothness and absence of stress concentrations.

Different shear stress distributions have been analyzed in detail. Apart from a distribution of the form of a hyperbolic sinusoid, corresponding to a constant-curvature cold-bent shape, the cases of linear, cubic and sinusoidal distributions have been considered. The hyperbolic sinusoid distribution is the one that, for fixed maximum deflection of the laminated glass beam, gives the most critical state of stress in the interlayer. The linear and cubic distributions give very similar results, both in terms of shear stress in the interlayer and axial stress in the glass plies.

But the form that presents the greatest advantages is the sinusoidal shear stress distribution. In fact, in this case there is no stress intensification in the neighborhood of the end of the beam, even when the shear modulus of the interlayer is high. In general, for the same sag of the laminated glass beam, the shear stress in the interlayer is lower than in the aforementioned cases, even if the maximum stress in the glass plies may be slightly higher at particular times of the history.

In any case, the differences in the deformed shapes of the laminated glass beam, associated with *all* the considered shear stress distributions, are minimal. Consequently, the aesthetics of the curved glazing is in practice not affected by any one of the proposed choices. This study has demonstrated that the constant-curvature shape should be avoided for cold-bending, because it is associated with noteworthy shear stress concentrations at the panel extremities, with consequent risk of delamination. The sinusoidal shape seems to be the optimal one, since it is associated with a smooth distributions of shear stress at any time of the element life.

Acknowledgements. Support of the European Community European Community under grant RFCS-RFSR-CT-2012-00026 "S+G" is gratefully acknowledged.

ABAQUS, 2010. Analysis users manual, version 6.10. Dassault systmes.

Barredo, J., Soriano, M., Gòmez, M.S., Hermanns, L., 2011. Viscoelastic vibration damping identification methods. Application to laminated glass. Procedia Eng. 10, 3208–3213.

Beer, B., 2013. Complex geometry facades - Introducing a new design concept for cold-bent glass, in: Proceedings of Glass Performance Days, Tampere (Finland).

Behr, R.A., Minor, J.E., Norville, H.S., 1993. Structural behavior of architectural laminated glass. J. Struct. Eng. 119, 202–222.

Belis, J., Inghelbrecht, B., Van Impe, R., Callewaert, D., 2007. Cold bending of laminated glass panels. Heron 52, 123–146.

Bennison, S., Sloan, J., Kristunas, D., Buehler, P., Amos, T., Smith, C., 2005. Laminated Glass for Blast Mitigation: Role of Interlayer Properties, in: Proceedings of Glass Performance Days, Tampere (Finland).

Bennison, S.J., Smith, C.A., Duser, A.V., Jagota, A., 2001. Structural performance of laminated glass made with a "stiff" interlayer, in: Proceedings of Glass Performance Days, Tampere (Finland).

Bennison, S.J., Stelzer, I., 2009. Structural properties of laminated glass., in: Short Course, Glass Performance Days, Tampere (Finland).

Eigensatz, M., Kilian, M., Schiftner, A., Mitra, N.J., Pottmann, H., Pauly, M., 2010. Paneling architectural freeform surfaces. ACM Trans. Graph. 29, 45:1–45:10.

Fildhulth, T., Knippers, J., 2011. Double curved glass shells from cold bent glass laminates, in: Proceedings of Glass Performance Days, Tampere (Finland), p. 384.

Fildhuth, T., Knippers, J., 2014. Interior stress monitoring of laminated cold bent glass with fibre bragg sensors, in: Proceedings of the Challenging Glass 4 and Cost Action TU0905 Final Conference, pp. 105–112.

Fildhuth, T., Knippers, J., Bindji-Odzili, F., Baldassini, N., Pennetier, S., 2014. Recovery behaviour of laminated cold bent glass-numerical analysis and testing, in: Proceedings of the Challenging Glass 4 and Cost Action TU0905 Final Conference, pp. 113–121.

Froli, M., Lani, L., 2011. Adhesion, creep and relaxation properties of PVB in laminated safety glass, in: Proceedings of Glass Performance Days, Tampere (Finland).

Galuppi, L., Massimiani, S., Royer-Carfagni, G., 2014. Buckling phenomena in double curved cold-bent glass. Int. J. Nonlinear Mech. 64, 70–84.

Galuppi, L., Royer-Carfagni, G., 2012a. Effective thickness of laminated glass beams. New expression via a variational approach. Eng. Struct. 38, 53–67.

Galuppi, L., Royer-Carfagni, G., 2012b. Laminated beams with viscoelastic interlayer. Int. J. Sol. Struct. 49, 2637–2645.

Galuppi, L., Royer-Carfagni, G., 2013. The design of laminated glass under time-dependent loading. Int. J. Mech. Sci. 49, 2637–2645.

Hooper, J.A., 1973. On the bending of architectural laminated glass. Int. J. Mech. Sci. 15, 309–323.

Ivanov, I.V., 2006. Analysis, modelling, and optimization of laminated glasses as plane beam. Int. J. Sol. Struct. 43, 6887–6907.

Kassnel-Henneberg, B., 2011. Purely structural glass building envelopes, in: Proceedings of Glass Performance Days, Tampere (Finland), p. 304.

Louter, C., Belis, J., Bos, F., Callewaert, D., Veer, F., 2010. Experimental investigation of the temperature effect on the structural response of sg-laminated reinforced glass beams. Eng. Struct. 32, 1590 – 1599.

Newmark, N.M., Siess, C.P., Viest, I.M., 1951. Tests and analysis of composite beams with incomplete interaction. Proc. Soc. Exp. Stress Anal. 9, 75–92.

Norville, H.S., King, K.W., Swofford, J.L., 1998. Behavior and strength of laminated glass. J. Eng. Mech. - ASCE 124, 46–53.

Pottmann, H., P, B., Schiftner, A., Schmiedhofer, H., Baldassini, N., Wallner, J., 2008. Architectural freeform structures from single curved panels. ACM Trans. Graphic. 27(3).

Timoshenko, S., MacCullough, G.H., 1949. Elements of Strength of Materials. Van Nostrad, New York.

de Vericourt, R., . Inextensional theory applied to cold bent glass built-in stress evaluation, in: Proceedings of Glass Performance Days, Tampere (Finland), p. 377.

Wiechert, E., 1893. Gesetze der elastischen nachwirkung für constante temperatur. Ann. der Phys. 286, 546–570.

Williams, M.L., Landel, R.F., Ferry, J.D., 1955. The temperature dependence of relaxation mechanisms in amorphous polymers and other glass-forming liquids. J. Amer. Chem. Soc. 77, 3701–3707.